

Accounts

Time-Resolved Total Internal Reflection Fluorometry Study on Chemical and Structural Characteristics at Water/Oil Interfaces

Shoji Ishizaka and Noboru Kitamura*

Division of Chemistry, Graduate School of Science, Hokkaido University, Kita-ku, Sapporo 060-0810

(Received May 15, 2001)

Structures and characteristics of water/oil interfaces at the molecular level are reviewed. Dynamic fluorescence anisotropy of Sulforhodamine 101 (SR101) and excitation energy transfer from SR101 to Acid Blue 1 (AB1) at water/oil interfaces were studied by using time-resolved total internal reflection (TIR) fluorometry. The results indicated that a water/carbon tetrachloride (CCl_4) interface was sharp with respect to the molecular size of SR101 ($\sim$10 Å), while a water/1,2-dichloroethane (DCE) interface was relatively rough compared to the water/CCl_4 interface. The present results were also compared with those predicted from molecular dynamic simulations and the thermally capillary wave theory. Furthermore, on the basis of fluorescence dynamic measurements of Sulforhodamine B (SRB) adsorbed at a water/oil interface, a relationship between thickness/roughness and the polarity at the interface was discussed.

Chemistry at a liquid/liquid interface is the fundamental basis for various sciences. In practice, it has been well recognized that an interface of two immisible liquid/liquid plays essential roles in chromatography, phase-transfer catalysis, solvent extraction, and other areas.[1–3] Furthermore, liquid/liquid interfacial systems have been also widely used in applied sciences (i.e., foods, photographs, paints, and cosmetics). Biological cells are an another example of liquid/liquid interfacial systems, in which two water phases are separated by an organic membrane wall and various chemical reactions proceed across the membrane wall. Therefore, directional mass/electron transfer across liquid/liquid interfaces has been studied as a model of biological systems.[4–18] Liquid/liquid interfacial systems have also been recently studied in reference to a model of molecular/ion recognition in biological systems.[19–21] All these interfacial phenomena are supposed to be dependent on the nature of a liquid/liquid interface, so that detailed understandings of chemical and structural characteristics of liquid/liquid interfaces at a microscopic level would afford wide benefit for further advances in various sciences. Nonetheless, very little is known about the chemical and structural characteristics of a liquid/liquid interface at a microscopic level.

So far, experimental studies on liquid/liquid interfaces have been conducted on the basis of thermodynamic,[22–24] spectroscopic,[25–32] and electrochemical techniques,[4–18] and fundamental knowledge about the properties of liquid/liquid interfaces has been accumulated over the past decades. However, experimental results obtained by these studies do not necessarily provide microscopic or molecular-level characteristics at the interface, since these studies are based essentially on bulk measurements. In the field of electrochemistry, as an example, mass/electron transfer processes across liquid/liquid interfaces have been studied extensively.[4–18] Although such approaches were very successful to elucidate kinetic mechanisms of interfacial processes, characteristic features of the chemistry at the interface in nanometer resolution cannot be obtained. One basic issue, which has thus remained unsolved, is the thickness and/or roughness at a liquid/liquid interface. For instance, Schiffrin and Girault studied ground-state electron transfer at a water/oil interface and reported that oil and water molecules were mixed in the interfacial region, which was thick enough to be considered as the third phase.[6] On the other hand, another view of the interface has been provided by a study on ion transfer kinetics across a water/oil interface by means of faradaic impedance measurements at equilibrium potentials. These studies predicted the existence of a "sharp inner layer" at the phase boundary.[7] To date, however, there is no clear experimental evidence for these models. A clearer picture of liquid/liquid interfacial phenomena is obtained only by exact knowledge about the structural characteristics at the interface. Experimental approaches other than those mentioned above are needed to reveal an unambiguous picture of the microscopic structures at a water/oil interface.

Recent advances in molecular dynamics simulations have provided invaluable information about molecular level characteristics at a water/oil interface.[33–41] As an example, Benjamin and his co-workers have reported the structures of water/carbon tetrachloride (CCl_4) and water/1,2-dichloroethane (DCE) interfaces on the basis of molecular dynamics computer simulations, and have demonstrated that a water/DCE interface is

molecularly sharp; there is no mixed solvent layer between the two phases.[33,34,36,39] However, they have also pointed out that the physical property of the interface is characterized by thermally capillary waves[42–45] generated at the interface and that the interface is quite rough on a short time scale. Such an information is very important to elucidate further the liquid/liquid interfacial structures, including their dynamics. Nonetheless, complementary studies by experiments are limited, so that the predictions given by the simulations are still controversial and worth checking experimentally.

Among the past decades, new experimental techniques were developed and applied to studying interfacial processes at a water/oil boundary: nonlinear optical techniques (second harmonic generation (SHG)[46–52] and sum frequency generation (SFG)),[53–65] X-ray reflectivity measurements,[66–68] quasi-elastic laser scattering (QELS),[69–74] and total-internal-reflection (TIR) spectroscopy.[75–93] Nonlinear optical techniques have afforded new insights about the characteristics at liquid/liquid interfaces, such as molecular orientations and hydrogen bonding structures of water. On the other hand, X-ray reflectivity measurements can afford information about the thickness of the interfacial layer. Nonetheless, it is very difficult to discuss dynamic motions of a molecule at the interface. QELS provides information about the role of thermal capillary waves in the physical properties of the interface. However, its time-resolution is in the rage of milliseconds so that dynamic aspects of the interfacial structures in nanometer scale cannot be obtained. On the other hand, it is well known that both nanometer and nanosecond–picosecond resolutions at an interface can be achieved by TIR fluorescence spectroscopy. Unlike steady-state fluorescence spectroscopy, fluorescence dynamics is highly sensitive to microscopic environments, so that time-resolved TIR fluorometry at water/oil interfaces is worth exploring to obtain a clearer picture of the interfacial phenomena.

One of the interesting targets to be studied is the characteristic of dynamic motions of a molecule adsorbed on a water/oil interface. Dynamic molecular motions at a liquid/liquid interface are considered to be influenced by subtle changes in the chemical/physical properties of the interface, particularly in a nanosecond–picosecond time regime, so that time-resolved spectroscopy is expected to be useful to study the nature of a water/oil interface.

We have studied water/oil interfaces on the basis of time-resolved total-internal reflection fluorescence spectroscopy and have discussed the structures and interfacial characteristics at a molecular level.[81,86,87,93] In these studies, we employed the following experimental approaches. One is a magic angle dependence of the TIR fluorescence decay profile of dye molecules adsorbed on a water/oil interface.[86,87,93] The other approach is a structural dimension analysis of excitation energy transfer dynamics between dye molecules adsorbed on a water/oil interface.[87,93] We applied these methods to studying water/oil interfaces, and succeeded in obtaining invaluable information on characteristic features at water/oil interfaces.

In this article, we review recent results on the studies of chemical and structural characteristics at water/oil interfaces with special references to those at water/CCl_4 and water/DCE interfaces. So far, water/CCl_4 and water/DCE interfaces have been studied by various techniques, and it has been reported that the water/CCl_4 and water/DCE interfaces are very thin: thickness of 1 nm.[33–41] Furthermore, molecular dynamics simulations reported by Michael and Benjamin indicate that the water/DCE interface is thicker and rougher compared to the water/CCl_4 interface.[39] Simulations give molecular-level insight about a liquid/liquid interface and are the indispensable basis for understanding the characteristics at the interface. Nonetheless, complementary studies by experiments are absolutely necessary, as mentioned above. Therefore, we explored picosecond TIR fluorescence spectroscopy to elucidate the structures of water/CCl_4 and water/DCE interfaces, and we compared the results with those predicted by molecular dynamics simulations.

1. A Magic-Angle Dependence of the TIR Fluorescence Decay Profile of SR101 at a Water/Oil Interface

Characteristics of a water/oil interface should appear in the molecular motions of a dye adsorbed on the interface. Wirth and Burbage reported in-plane and out-of-plane reorientation dynamics of Acridine Orange at water/oil interfaces on the basis of fluorescence depolarization measurements and, demonstrated that out-of-plane reorientation of the dye was influenced by surface roughness, while the in-plane reorientational dynamics was almost independent of the viscosity of the oil phase.[76] Although a fluorescence depolarization technique is certainly promising to obtain an inside look at a liquid/liquid interface, the number of such studies is still limited. In order to obtain more detailed information, we therefore conducted TIR fluorescence dynamic anisotropy measurements of a dye adsorbed on water/oil interfaces on the basis of a picosecond time-correlated single photon counting technique.[86,87,93]

For TIR fluorescence spectroscopy on water/oil interfaces, the choice of a probe molecule is of primary importance. For example, the penetration depth (d_p) of an incident evanescent wave at a DCE (refractive index (n); $n_1 = 1.44$)/water ($n_2 = 1.33$)[94] interface is calculated to be ~94 nm on the basis of the equation, $d_p = \lambda/\{4\pi(n_1^2\sin^2\theta_i - n_2^2)^{1/2}\}$, where λ is the wavelength (580 nm) of an excitation laser beam and θ_i is the incident angle of the laser beam (80°).[75] It has been reported that the thickness of a sharp water/oil interface represented by water/DCE is ~1 nm,[33] so that d_p of the incident evanescent wave is thicker than the thickness of the interfacial layer, and the fluorescence characteristics of a probe molecule in the bulk phase are superimposed, more or less, on those at the interface.[81] Therefore, a probe molecule should be highly surface active and adsorb on the interface, so as to exclude fluorescence of the probe molecule from the bulk phase. In the present experiments, we employed Sulforhodamine 101 (SR101) as a fluorescence probe throughout the study, since SR101 is highly surface active and adsorbs strongly on a water/oil interface. This has been confirmed by interfacial tension (γ) measurements reported elsewhere.[86,87] The structures and abbreviations of the dye molecules used in this study are shown in Scheme 1.

Dynamic fluorescence anisotropy is based on rotational reorientation of the excited dipole of a probe molecule, and its correlation time(s) should depend on local environments around the molecule. For a dye molecule in an isotropic medium, three-dimensional rotational reorientation of the excited

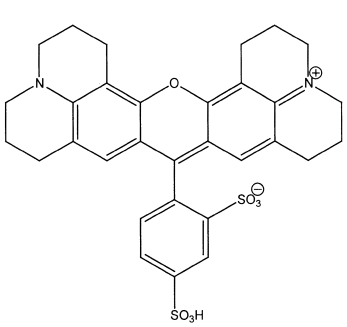

Sulforhodamine 101 (SR101)

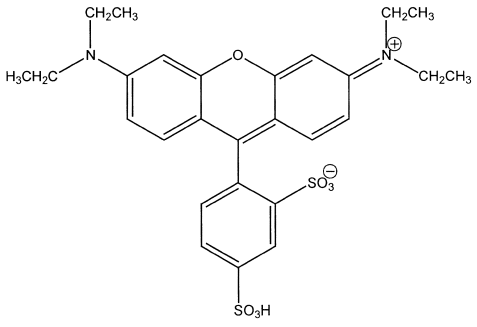

Sulforhodamine B (SRB)

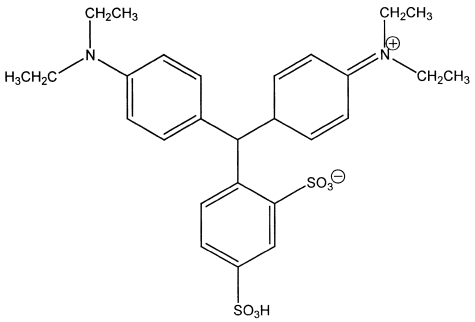

Acid Blue 1 (AB1)

Scheme 1. Structures and abbreviations of the dye molecules used in this study. (a) Sulforhodamine 101; SR101, (b) Sulforhodamine B; SRB, (c) Acid Blue 1; AB1.

dipole takes place freely.[95] At a water/oil interface, on the other hand, the out-of-plane motion of a probe molecule should be frozen when the dye is adsorbed on a sharp water/oil interface (i.e., two-dimensional in respect to the molecular size of a probe), while such motion will be allowed for a relatively thick water/oil interface (i.e., three-dimensional).[77,96] Thus, by observing rotational freedom of a dye molecule (i.e., excited dipole), one could discuss the thickness of a water/oil interface; the correlation time(s) provides information about the chemical/physical characteristics of the interface, including the dynamical behavior of the interfacial structure. Dynamic fluorescence anisotropy measurements are thus expected to provide new insights about a water/oil interface, not obtained by conventional spectroscopies.

The laboratory coordinate system chosen for TIR fluorescence anisotropy measurements is illustrated in Fig. 1. SR101 molecules located at a water/oil interface (in the X–Y plane) are excited by an s-polarized laser beam along the X-axis. The TIR fluorescence is then detected along the Z-axis and its polarization is selected by a polarizer. The fluorescence decay profile observed under such a configuration is analyzed for two limiting cases, depending on the structure of a water/oil interface: two-dimensional or three-dimensional.

Case I: Two-Dimensional Model. If the thickness of a water/oil interface is comparable to the molecular size of SR101 and the dye molecules located at the interface are strongly oriented, the rotational motions of SR101 will be

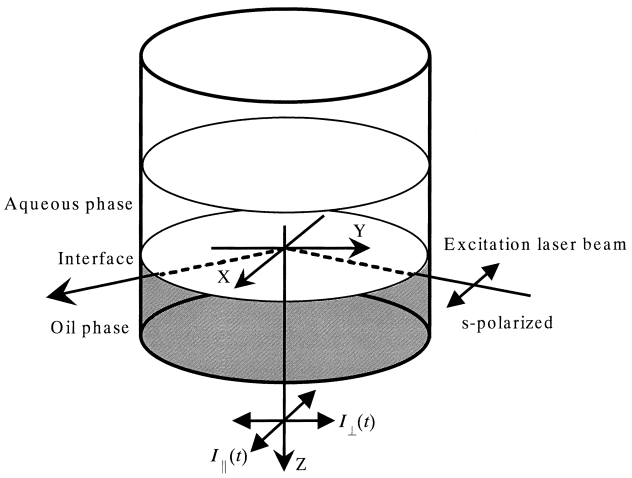

Fig. 1. Coordinate system defined in the experiment. The X–Y plane is the plane of the interface.

strongly restricted in the interfacial layer (X–Y plane of the interface, two-dimension), and the emission dipole moment of SR101 (direction of the long axis of the xanthene ring) directs within the X–Y plane. In such a case, the time profile of the total fluorescence intensity of SR101 observed from the interface should be proportional to $I_{\parallel}(t) + I_{\perp}(t)$, where $I_{\parallel}(t)$ and $I_{\perp}(t)$ represent the fluorescence decay profiles observed with emission polarization parallel and perpendicular to the direc-

tion of excitation polarization, respectively. When the angle of the emission polarizer is set at 45° with respect to the X axis (magic angle), fluorescence anisotropy is canceled, so that the TIR fluorescence decay curve can be analyzed by a single-exponential function. If a water/oil interface is very sharp, therefore, fluorescence dynamic anisotropy $r(t)$ obeys Eq. 1,

$$r(t) = \frac{I_{\parallel}(t) - I_{\perp}(t)}{I_{\parallel}(t) + I_{\perp}(t)} = r(0)\exp\left(-t/\tau^{rot}\right) \quad (1)$$

where $r(0)$ and τ^{rot} are initial anisotropy ($t = 0$) and the reorientation correlation time, respectively. In Case I, $r(0)$ should be equal to 0.5.[96]

Case II: Three-Dimensional Model. On the other hand, if the interfacial layer is thick enough compared to the molecular size of SR101 and if SR101 molecules adsorbed on the interface are weakly oriented, the rotational motions of SR101 take place in three dimensions, similar to those in a bulk phase. If this is the case, the contribution of the fluorescence with the excited dipole moment of SR101 directed along the Z axis cannot be neglected, so that the time profile of the total fluorescence intensity must be proportional to $I_{\parallel}(t) + 2I_{\perp}(t)$. Thus, fluorescence dynamic anisotropy is given by Eq. 2, as is well known for that in a macroscopically isotropic system:[95,97]

$$r(t) = \frac{I_{\parallel}(t) - I_{\perp}(t)}{I_{\parallel}(t) + 2I_{\perp}(t)} = r(0)\exp\left(-t/\tau^{rot}\right) \quad (2)$$

and $r(0)$ and the magic angle are calculated to be 0.4 and 54.7°, respectively. The thickness of a water/oil interfacial layer would be evaluated through TIR fluorescence anisotropy measurements and the τ^{rot} value(s) provides information about characteristic features of a water/oil interface.

Fluorescence dynamic anisotropy measurements under normal (bulk) or TIR conditions were conducted as described previously.[86,87,93] Briefly, an excitation laser beam, polarized perpendicular to the plane of incidence (s-polarized) by using a Glan-laser prism, was irradiated to a water/oil interface through the oil phase, as illustrated in Fig. 2. In the present experiments, the incident angle of the laser beam (θ_i) was set (80°) larger than the critical total-reflection angle at the water/oil interface. The fluorescence from the sample was collected along the surface normal and its polarization was selected with a polarizer (Polaroid, HNP'B). The polarized fluorescence was detected by a microchannel-plate photomultiplier (Hamamatsu, R3809U-50) equipped with a monochromator (Jobin Ybon, H-20) and analyzed by a single-photon counting module (Edinburgh Instruments, SPC-300). All experiments were conducted at room temperature (~23 °C).

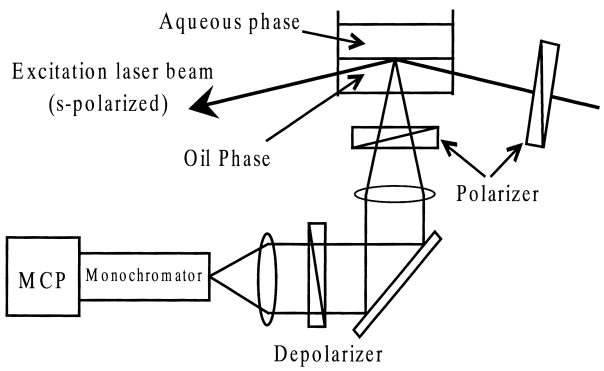

Fig. 2. Schematic illustration of a system for total internal reflection fluorescence dynamic measurements at water/oil interface.

We studied water/phthalate ester (PE) interfacial systems.[86] In bulk homogeneous solutions, SR101 exhibited a single rotational reorientation time in the range of 0.21–12.9 ns, depending on the viscosity of the medium (0.93–70.7 cP at 23 °C). At a water/PE interface, on the other hand, fluorescence anisotropy of the dye showed a double exponential decay with the time constants of 0.27–0.89 and 1.38–3.30 ns; these values varied with the structure of the ester alkyl groups in PE. Since the rotational reorientation times observed at the interface agree with neither the value in water (0.21 ns) nor that in the relevant bulk oil solution, the water/PE interfacial structure is concluded to be much different from that in each phase. The observed rotational reorientation times of the dye provided molecular-level information about specific adsorption modes of SR101 on water/PE interfaces. Furthermore, rotational freedom of SR101 observed at the interface was two-dimensional like, so that the water/PE interface was concluded to be sharp in respect to the molecular size of SR101 (~1 nm). The present approach was shown to be one potential means to discuss the thickness of the interfacial layer in the spatial resolution of the order of ~1 nm.

The experimental idea was then applied to study water/CCl_4 and water/DCE interfacial systems.[87] Figure 3 shows fluorescence decay profiles of SR101 observed from water/CCl_4 and water/DCE interfaces at an emission polarization angle of 45° ((a) and (c)) or 54.7° ((b) and (d)), together with the relevant weighted residuals (*Re*) and autocorelation trace (*Cr*) for each single-exponential fit. In the case of the water/CCl_4 interface ((a) and (b)), *Re* and *Cr* of the data observed at 54.7° exhibited nonrandom distributions compared to those predicted by the best fit (b), particularly, those in the initial stage of excitation (< 1 ns). But, the profile observed at the magic angle 45° was reasonably fitted by a single exponential function as judged by the relevant *Re* and *Cr* (a).[95] The χ^2 and Durbin–Watson (DW) parameters for the fitting also support that the best fit of the observed data by a single-exponential function is attained by setting an emission polarizer at the magic angle, 45° (Table 1). Therefore, it is concluded that the water/CCl_4 interface is sharp with respect to the molecular size of SR101 and that three-dimensional rotational motions of SR101 are inhibited at the water/CCl_4 interface.

In the case of a water/DCE interface ((c) and (d)), on the other hand, a fitting of the data by a single exponential function cannot be attained by setting an emission polarizer at 45°, as confirmed by deviations of *Re* and *Cr* from the optimum values (c). When the fluorescence decay profile is measured by setting an emission polarizer at 54.7° (d), fluorescence anisotropy can be reasonably fitted by a single exponential function including the time response in the initial stage of excitation (see also χ^2 and DW in Table 1). Therefore, the interfacial layer of the water/DCE interface is thick compared to the molecular size of SR101, and the dye molecules adsorbed on the interface are weakly oriented. Otherwise, the interface is

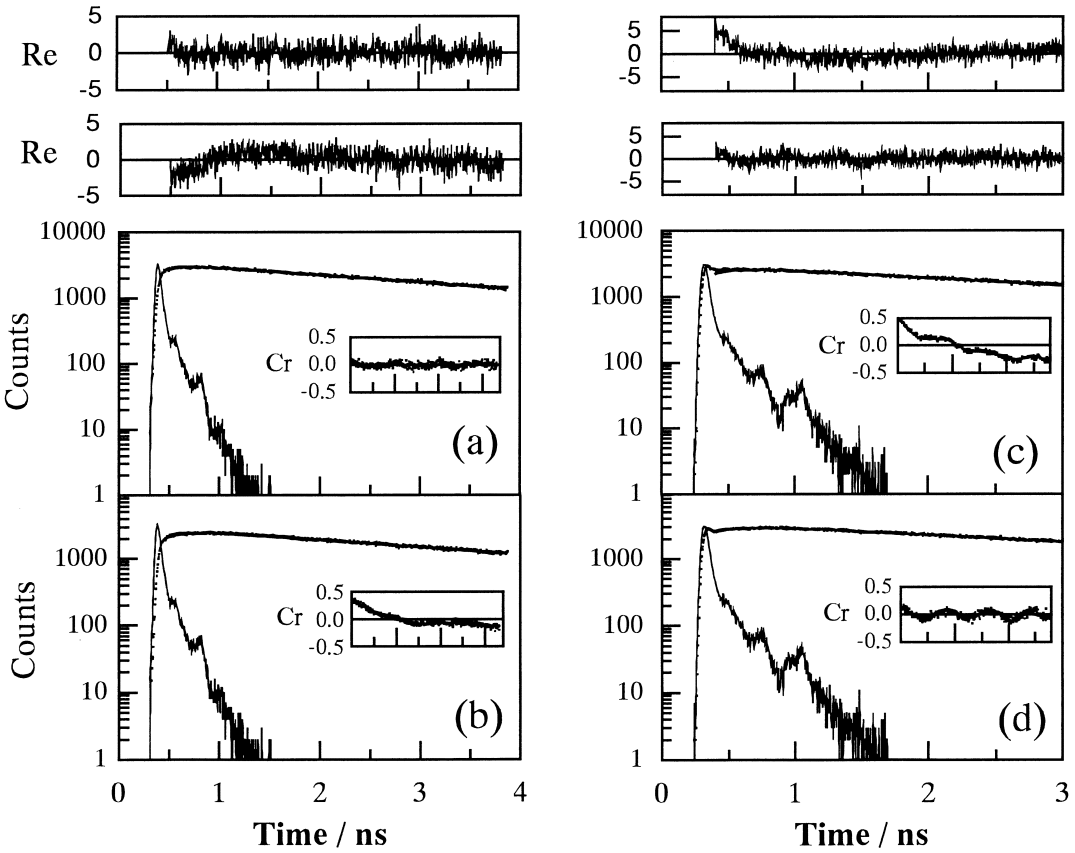

Fig. 3. TIR fluorescence decay curves of SR101 at water/CCl_4 ((a) and (b)) and water/DCE ((c) and (d)) interfaces. The angle of the emission polarizer 45° was set ((a) and (c)) or 54.7° ((b) and (d)) in respect to the direction of excitation polarization. The upper and inner panels of each figure represent the plots of the weighted residuals (*Re*) and the autocorelation trace (*Cr*) for a single-exponential fitting, respectively.

Table 1. Fluorescence Decay Parameters of SR101 Adsorbed on Water/Oil Interfaces Observed under the TIR Conditions and in an Aqueous Solution

		τ/ns	χ^{2} a)	DW a)
Water/CCl_4	45° b)	4.06 ± 0.02	1.11	1.88
	54.7° b)	4.21 ± 0.03	1.61	1.37
Water/DCE	45° b)	3.62 ± 0.02	2.28	0.90
	54.7° b)	4.12 ± 0.03	1.09	1.73
aq c)		4.12 ± 0.01	1.16	1.94

a) χ^2 and DW represent the χ^2 and Durbin–Watson parameters for the fitting, respectively.
b) The angle of the emission polarizer in respect to that of the excitation laser beam.
c) Determined in an aqueous SR101 solution ([SR101] = 1.7×10^{-7} M).

spatially rough at the molecular size of SR101. SR101 molecules at the water/DCE interface behave similar to those in an isotropic medium, in contrast to the results at the water/CCl_4 interface.

2. Excitation Energy Transfer and Its Dynamics at a Water/Oil Interface

It is worth noting that water/oil interfacial structures would be governed by various factors, so that a complementary study other than fluorescence dynamic anisotropy is required to obtain further detailed information about the characteristics at a watre/oil interface. As a new and novel approach, therefore, excitation energy transfer dynamics and the relevant structural (fractal) dimension analysis were introduced to elucidate the structure of a water/oil interface.

Sitzmann and Eisenthal reported excitation energy transfer from Rhodamine 6G to 3,3′-diethyloxadicarbocyanine iodide at an air/water interface on the basis of time-resolved second harmonic generation measurements. They demonstrated that excitation energy transfer dynamics at the interface could be analyzed by a two-dimensional model.[98] In their measurements, nonetheless, the signal-to-noise ratios of the measurements were not necessarily good, so that the discussions are still controversial.

We consider here dipole–dipole (Förster-type) excitation energy transfer between an energy donor (D) and an acceptor (A) both adsorbed on a water/oil interface. When diffusional motions of D and A are inhibited, as in the case for strong binding of the molecules to the surface by adsorption, excitation energy transfer quenching dynamics of D by A reflects structural dimension around D and A through spatial distributions of the components.[99] Actually, the method has been applied to study nanometer-scale morphologies in Langmuir–Blodgett films,[100,101] vesicles,[101,102] polymers,[103–106] and silica gels.[107–109] In such a case, fluorescence dynamics of D ($I_D(t)$) should obey

the following equation, as reported by Klafter and Blumen,[99]

$$I_D(t) = A \exp\left(-(t/\tau_D) - P(t/\tau_D)^{\bar{d}/6}\right) \quad (3)$$

where A is a pre-exponential factor and τ_D is the excited state lifetime of D without A. P is a parameter proportional to the probability that A resides within the critical energy transfer distance (R_0) of the excited donor. $\bar{d}$ is called the fractal dimension and reflects a spatial distribution of A around D. If D and A molecules adsorb uniformly on a sharp water/oil interface (two-dimensional), $\bar{d}$ should be 2.0, since excitation energy transfer takes place exclusively along the lateral direction at the interface. On the other hand, if a water/oil interface is thick and rough in respect to the molecular size of a probe molecule, $\bar{d}$ should be 2.0–3.0, since the possibility of energy transfer along the direction other than the lateral direction cannot be neglected. Therefore, we expect that a study on excitation energy transfer dynamics will provide invaluable information about the characteristics at a water/oil interface, along with a complementary study on the same system by fluorescence dynamic anisotropy.

Figure 4 shows the fluorescence and absorption spectra of SR101 (donor) and Acid Blue 1:AB1 (acceptor) in water, respectively. As seen in Fig. 4, since the fluorescence spectrum of SR101 overlaps with the absorption spectrum of AB1, effective excitation energy transfer from SR101 to AB1 is expected. In the present case, energy transfer between the excited singlet state of SR101 and AB1 proceeds via a Förster-type mechanism,[110] so that the energy transfer efficiency can be estimated by the following equation:

$$R_0^6 = \frac{9000\ln(10)\kappa^2\phi_0}{128\pi^5 n^4 N_A} \int_0^\infty \frac{F_D(\nu)\varepsilon_A(\nu)}{\nu^4}\, d\nu \quad (4)$$

In Eq. 4, R_0 is the critical energy transfer distance and κ is an orientational factor for energy transfer (usually assumed to be $\kappa^2 = 2/3$). ϕ_0 is the fluorescence quantum yield of the donor in the absence of an acceptor and n is the refractive index of the medium. N_A, $F_D(\nu)$, and $\varepsilon_A(\nu)$ are the Avogadro's number, the spectral distribution of the fluorescence in quanta normalized to unity, and the molar absorptivity of AB1 at each wavenumber ν, respectively. According to Eq. 4, R_0 in water is calculated to be 71 Å,[111] indicating that efficient excitation energy transfer from SR101 to AB1 should occur. Therefore, on the basis of analysis of fluorescence decay curves of SR101 at a water/oil interface in the presence of AB1, the structure of the interface could be estimated with the spatial resolution being in the order of R_0 (~70 Å).

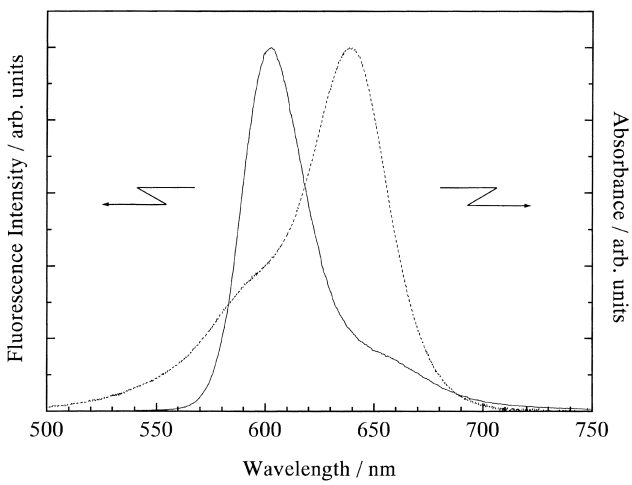

Fig. 4. Fluorescence spectrum of SR101 (solid line) and absorption spectrum of AB1 (dashed line) in water.

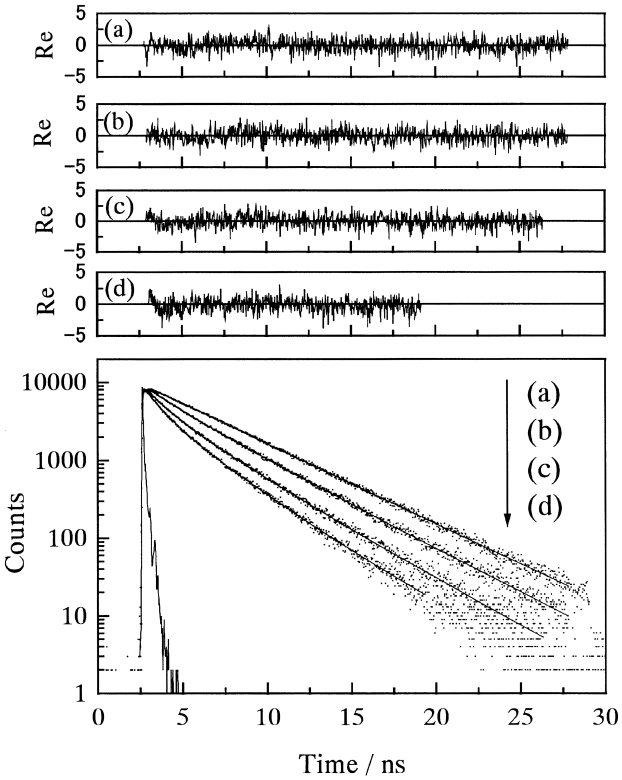

Fig. 5. Fluorescence decay profiles of SR101 at a water/DCE interface in the absence and presence of AB1: (a) [AB1] = 0, (b) 1.91×10^{-9}, (c) 3.82×10^{-9}, (d) 5.73×10^{-9} M. The solid curve shows the best fit by Eq. 3. The fastest decay profile denotes an instrumental response.

Figure 5 shows the fluorescence decay curves of SR101 at a water/DCE interface in the absence ((a)) and presence of AB1 (1.91, 3.82, and 5.73×10^{-9} M for (b), (c) and (d), respectively). Analogous results were obtained for a water/CCl_4 system (data are shown elsewhere).[87] In the absence of AB1, the fluorescence decay of SR101 was fitted satisfactorily by a single-exponential function with the decay time of 4.21 ns. In the presence of the acceptor, on the other hand, the fluorescence exhibited a non-single exponential decay. For energy transfer dynamics in fixed geometries of both energy donor and acceptor, the fluorescence decay profile of the donor cannot be expressed by a single exponential function, but should be analyzed by a Klafter–Blumen equation (Eq. 3) as demonstrated for that in various inhomogeneous systems.[99,100,103,105] In Eq. 3, $\bar{d}$ is the structural (fractal) dimension as described before and, in the present case, this reflects the spatial distribution of AB1 around SR101 at a water/CCl_4 or water/DCE interface. P is the term related to the AB1 concentration at a water/oil inter-

face, which is defined by Eq. 5.

$$P = \theta_A(d/\overline{d})\Gamma(1-\overline{d}/6)(R_0/a)^{\overline{d}} \quad (5)$$

In Eq. 5, θ_A is the degree of interfacial coverage of AB1 and d is an Euclidean dimension (2, in the case of surface adsorption). a is the effective radius of SR101 (7 Å). Γ represents a gamma function. Simulations of the observed decay profiles in Fig. 5 were then performed on the basis of Eq. 3 with τ_D being fixed at 4.21 ns. The parameters obtained by the simulation (P and $\overline{d}$) are summarized in Table 2, together with the χ^2 parameters of the fittings. The χ^2 parameters and the weighted residuals (Re) of the fittings, shown in the upper traces of Fig. 5, indicate that the fluorescence decay profiles of SR101 are well fitted by Eq. 3.

Although statistical validity of the fitting can be judged by χ^2 and Re, the application of the Klafter–Blumen equation to the decay profile analysis is not necessarily warranted and is worth checking in more detail. First, the Klafter–Blumen model requires that the fluorescence decay profiles observed at different AB1 concentrations should be fitted by a common $\overline{d}$ value. As shown in Table 2, this requirement is safely satisfied; the $\overline{d}$ value for the water/CCl_4 or water/DCE system was 1.86–2.00 or 2.45–2.53, respectively, which was within the experimental errors.

According to Eq. 5, second, the P value obtained by the fitting should increase linearly with an increase in the degree of interfacial coverage (θ_A) of AB1 on the water/oil interface. In order to estimate θ_A, therefore, interfacial tension (γ) measurements were conducted. The relationship between P and θ_A thus obtained is shown in Fig. 6. It is worth noting that the P value increases linearly with an increase in θ_A for both cases. The results demonstrate explicitly that the Klafter–Blumen model in Eqs. 3 and 5 is applicable to the present system. Furthermore, the dye concentration adsorbed on the interface is very low (interfacial coverage of AB1: 0.12–1.51%, SR101: 0.06–0.29%) so that the interfacial structure is not influenced appreciably by dye adsorption. Therefore, the variation of the $\overline{d}$ value with the nature of the oil (Table 2) is meaningful and is worth discussing in detail.

The results in Fig. 6 also provide information about the critical energy transfer distance between SR101 and AB1 at the water/oil interface. Knowing d, $\overline{d}$, and a, one can calculate the

Table 2. Structural Dimension Analysis of Excitation Energy Transfer Quenching of SR101 by AB1 at the Water/Oil Interfaces

	[AB1]/10^{-9} M	P [a)]	$\overline{d}$[b)]	χ^2
Water/CCl_4	1.91	0.82	1.86	1.06
	3.82	1.46	1.94	1.00
	5.73	1.97	2.00	1.01
Water/DCE	1.91	0.50	2.47	1.05
	3.82	1.06	2.45	1.05
	5.73	1.40	2.53	1.15

a) The P parameter defined in Eq. 5.

b) The structural dimension determined by excitation energy transfer quenching of SR101 fluorescence by AB1 (see main text).

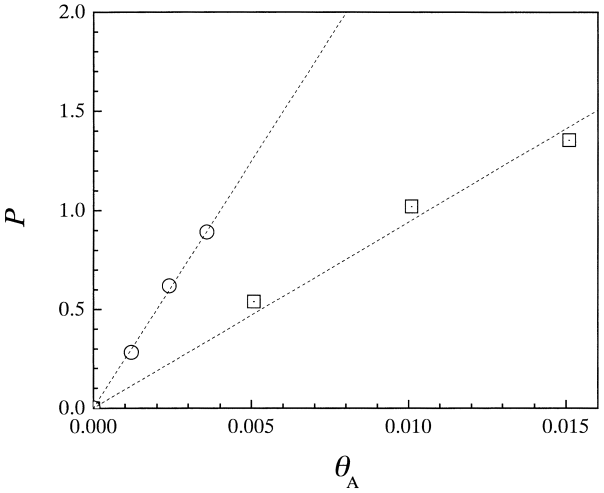

Fig. 6. Relationship between P and θ_A, for water/CCl_4 (open square) and water/DCE systems (open circle). The dashed line represents the best fit by using Eq. 5.

R_0 value on the basis of the slope value of the plot in Fig. 6 and Eq. 5. Actually, the R_0 value at the water/CCl_4 or water/DCE interface was calculated to be 75 or 74 Å, respectively. These R_0 values are comparable to that (71 Å) estimated from Eq. 5. This also supports validity of the present analysis by the Klafter–Blumen model in Eq. 3.

The structural dimension for energy transfer at the water/CCl_4 or water/DCE interface (Table 2) was 1.86–2.00 (average, 1.93) or 2.45–2.53 (2.48), respectively. The present Klafter–Blumen analysis of the data is very meaningful as described above, so that structural characteristics of the interface should be reflected on the $\overline{d}$ value. The $\overline{d}$ value for the water/CCl_4 interface (1.93) indicates that the interface is sharp and can be regarded as two-dimensional, for the spatial resolution by the energy transfer quenching method (~70 Å or ~7 nm). Phenomenologically, the result agrees well with that derived from fluorescence dynamic anisotropy measurements; the interface is thin enough to inhibit three-dimensional rotational motions of SR101. If the interface is thin enough and modeled strictly by two-dimensions, however, the structural dimension should be equal to 2.0, since energy transfer quenching is restricted in the X–Y plane of the interface. A $\overline{d}$ value smaller than 2.0 has frequently been reported for the interfacial systems such as vesicles and Langmuir–Blodgett films, and $\overline{d} <$ 2.0 in these systems has been discussed in terms of a non-uniform distribution of an energy acceptor at the interface: fractal structure.[100,101] Therefore, a fractal-like distribution of AB1 at the water/CCl_4 interface might play a role in deciding the $\overline{d}$ value.

On the other hand, the structural dimension determined for the water/DCE interface was larger than 2.0:2.48. This suggests that the water/DCE interface is thicker than the water/CCl_4 interface. The fluorescence dynamic anisotropy measurements also gave analogous results; the interface is thick enough to allow three-dimensional rotational motions of SR101. It should be noted that these results do not necessarily imply that the water/DCE interface is characterized by a three-dimensional space. Taking the results obtained by molecular dynamics simulations into account, it is supposed that the wa-

ter/DCE interface is thin, but is rough in respect to the spatial resolution by the energy transfer quenching method, as discussed in the following section.

3. Structures of Water/Oil Interfaces

3.1 Water/CCl_4 and Water/DCE Interfaces. In the present study, both fluorescence dynamic anisotropy and excitation energy transfer methods were successful in providing information about the structures and thickness/roughness of the water/CCl_4 and water/DCE interfaces. However, it should be noted that, although the results obtained by the present two methods are complementary to discuss the structures of the interfaces, these cannot be compared directly with each other, since fluorescence dynamic anisotropy provides information about molecular level structures of the interface (i.e., dimension of the molecular size of SR101 $\sim$1 nm) while the excitation energy transfer method affords relatively long-range interfacial structures (i.e., dimension of the critical energy transfer distance $\sim$7 nm). On the basis of such experimental backgrounds, the following discussions are offered.

A water/CCl_4 or water/DCE interface is a representative system studied by various techniques; so far, invaluable information about the structure of the interface has been accumulated.[33–41] As an example, Benjamin and his co-workers have demonstrated that a water/DCE interface is molecularly sharp; there is no-mixed solvent layer between the two phases.[33,34,36,39] However, they have also pointed out that the physical property of the interface is characterized by thermally capillary waves generated at the sharp interface and that the interface is quite rough at a short time scale.[5,34] According to their calculations, namely, the capillaries with the amplitude as short as 0.8 nm are constantly moving at the interface and these protrude into the DCE phase on the time scale of tens of picoseconds. However, the long time average (hundreds of picoseconds) of the interface results in a relatively smooth density profile that gives rise to the interface thickness of about 1 nm. Molecular dynamics simulations and interfacial tension measurements have also demonstrated that the water/CCl_4 interface is thinner than the water/DCE interface; the thickness of the water/CCl_4 interface has been reported to be $<$ 1 nm.[39] Molecular dynamics simulations provides information about molecular level structures of the interface. The spatial resolution of fluorescence dynamic anisotropy measurements is $\sim$1 nm (i.e., the dimension of the molecular size of SR101), so that the present results are worth comparing with the predictions from the simulations.

The thickness of the water/DCE interface (1 nm) is comparable to the molecular size of SR101 (1.0–1.4 nm).[86] Furthermore, SR101 molecules adsorbed on the water/DCE interface are supposed to be restricted within the two-dimensional plane, with the hydrophilic SO_3^- group being towards to the water phase while the hydrophobic xanthene ring is directed to the DCE phase.[86] Therefore, when the water/DCE interface is very sharp, three-dimensional-like rotational reorientation of SR101 would not be observed, in contrast to our experimental observation. One possible reason for this is thermal fluctuations of the interface, by which SR101 molecules behave similar to those in an isotropic medium: SR101 on the interface are tumbled by thermal fluctuations. Similar situations are also expected for SR101 at the water/CCl_4 interface, while the dynamic anisotropy experiments suggest that the interface is two-dimensional-like. It has been reported that thermal capillary waves at an interface are related to the interfacial tension of the system.[42–45] In the present systems, the lower interfacial tension of the water/DCE system compared to that at the water/CCl_4 interface indicates that the amplitude(s) of the surface wave(s) is larger for the water/DCE system relative to that for the water/CCl_4 interface. This prediction agrees with the results from the computer simulations as described above; the thickness of the water/DCE or water/CCl_4 interface is 1 nm or $<$ 1 nm, respectively. Thus, the contribution of the thermal fluctuation to the rotational motions of SR101 would be smaller at the water/CCl_4 interface, leading to a two-dimensional-like anisotropy decay of the dye at the interface.

Short-range ($\sim$1 nm) structural information about the interface obtained by fluorescence dynamic anisotropy experiments is not contradicted by the results by the excitation energy transfer method: $\overline{d}$ (water/CCl_4) = 1.93 and $\overline{d}$ (water/DCE) = 2.48. Energy transfer at a water/oil interface is schematically shown in Scheme 2. For simplicity, it is assumed here that an SR101 molecule (closed circle) sits on the interface (X–Y plane). The molecular size of SR101 is 1.4 nm and the critical energy transfer distance is $\sim$7 nm, so that energy transfer proceeds at a long distance. When both SR101 and AB1 are located at a flat interface, the structural dimension of energy transfer should be exactly 2.0. If the interface is rough and AB1 (closed triangle in Scheme 2) is displaced from the X–Y plane, on the other hand, the angle between the positions of the SR101 and AB1 molecules along the Z axis (φ in Scheme 2) determines the $\overline{d}$ value. Clearly, when displacement along the Z axis (δ) is very small, $\overline{d}$ is 2.0. An increase in δ implies that the interface becomes rougher and, thus, $\overline{d}$ increases to 3.0. Since SR101 at the water/DCE interface exhibits three-dimensional-like motions, the interface has been suggested to be rougher compared to the water/CCl_4 interface. Therefore, the structural dimension of the water/DCE interface ($\overline{d}$ = 2.48) will be a reasonable consequence, reflecting the characteristic structure of the interface.

In the above experiments, we used SR101 as a probe molecule, since the nonradiative decay rate constant is not sensitive to solvation environments owing to the ring structure in the xanthene chromophore.[113] Actually, the fluorescence lifetime of SR101 at a water/oil interface was identical to that in an aqueous solution, as shown in Table 1. On the other hand, the

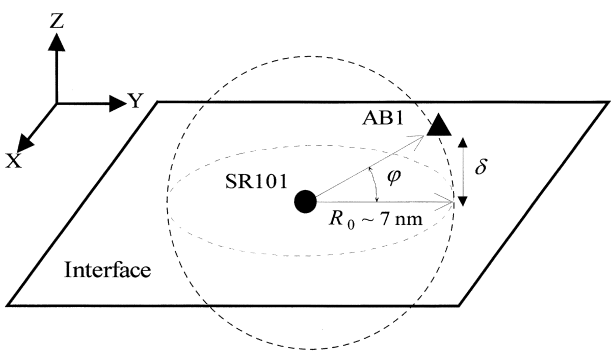

Scheme 2.

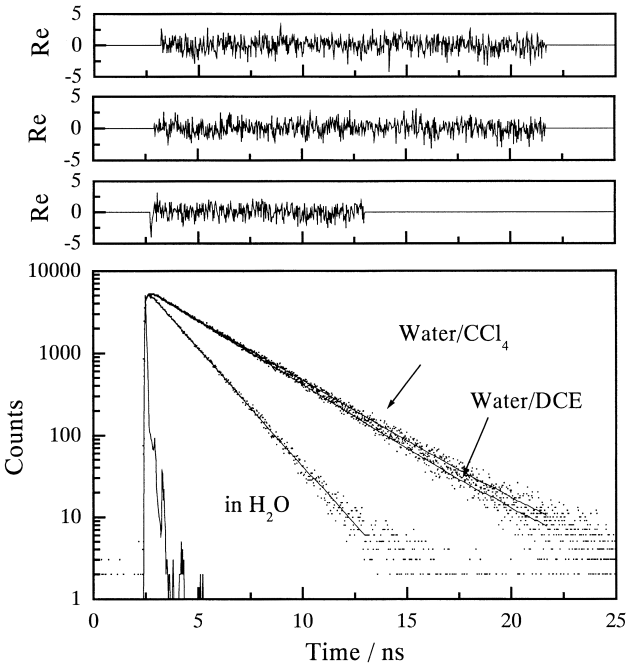

Fig. 7. Fluorescence decay profiles of SRB at a water/CCl_4 interface, a water/DCE interface and in water. The solid curve shows the best fit by a single-exponential function. The upper panels of the figure represent the plots of the weighted residuals (*Re*) for a single-exponential fitting.

diethylamino group in Sulforhodamine B (SRB) can rotate freely, and the nonradiative decay rate constant of the molecule is sensitive to solvent polarity. Figure 7 shows the fluorescence decay profiles of SRB at a water/DCE interface and in an aqueous solution, together with the relevant *Re* for each single-exponential fit. It is noteworthy that the TIR fluorescence decay curve observed at a water/DCE interface is reasonably fitted by a single-exponential function as judged by *Re*, and the lifetime at the interface is longer than that in an aqueous phase (1.5 ns). The single-exponential fit indicates that the local solvation structure around SRB is common for almost all the dye molecules adsorbed on the interface. As discussed in the preceding section, nonetheless, the structural dimension at a water/DCE interface is larger than 2, demonstrating that excitation energy transfer quenching of the SR101 fluorescence takes place other than in the lateral direction (X–Y plane). If the water/oil interfacial layer is thick (> 1 nm) and the water/oil composition varies gradually within the layer, the TIR fluorescence of SRB should decay multi-exponentially, reflecting various solvation structures around SRB at the interface. On the other hand, short-range structural information about the interface obtained by the fluorescence dynamic anisotropy experiments suggested that the interface was three-dimensional-like. These results can be understood only by the fact that the water/DCE interface is thin (~1 nm), but is rough with respect to the spatial resolution of the excitation energy transfer quenching method (~7 nm), as shown in Scheme 3.

Although the structural differences between the water/CCl_4 and water/DCE interfaces are not so large, the chemical and/or physical nature of the organic phase itself reflects on the photophysical properties of a probe molecule, indicating the novelty of the present experimental approaches. Systematic investigations on liquid/liquid interfaces are important to reveal factors governing structural and physical characteristics of liquid/liquid interfaces. Therefore, we introduced fluorescence dynamic anisotropy and excitation energy transfer measurements to several water/oil interfacial systems; the data are summarized in Table 3. The results are discussed in terms of the relationship between the interfacial structure and polarity at water/oil interfaces (section 4).

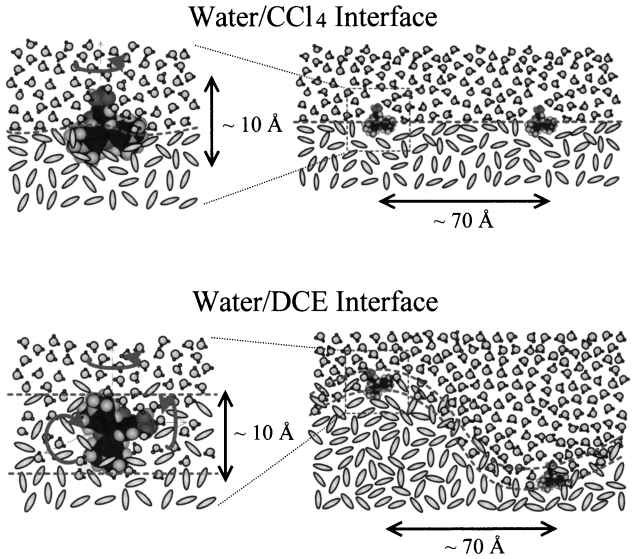

Scheme 3.

Table 3. Magic-Angles for the TIR Fluorescence Anisotropy Measurements and Structural Dimensions at the Interfaces

Org. Phase	γ[a] /mN m^{-1}	aq in[b] /wt%	in aq[b] /wt%	Magic angle[c]	$\bar{d}$[d]
Cyclohexane	51[e]	0.01	0.006	45°	1.90
CCl_4	45	0.01	0.08	45°	1.93
Toluene	33	0.03	0.05	~45°	2.13
CB[f]	37	0.03	0.05	~45°	2.20
DCB[f]	39	0.31	0.03	45–54.7°	2.30
DCE	28	0.15	0.81	~54.7°	2.48

a) Interfacial tension of the water/oil system, determined by a pendant drop method.[112]
b) Taken from Ref. 94
c) The angle of an emission polarizer, by which the fluorescence decay is best fitted by a single-exponential function.
d) The structural dimension determined by excitation energy transfer quenching of SR101 fluorescence by AB1 (see main text).
e) Ref. 114.
f) CB and DCB represent chlorobenzene and *o*-dichlorobenzene, respectively.

3.2 Theoretical Considerations. The simplest way to understand the difference in the interfacial structure will be to consider the interfacial tension. An interfacial tension (mN m^{-1}) is equivalent to an interfacial free energy (mJ m^{-2}).[114] As shown in Table 3, the interfacial free energy in the water/CCl_4 system (44.5 mJ m^{-2}) is higher than that in the water/DCE system (27.9 mJ m^{-2}). The energy necessary to construct a water/

CCl_4 interface is larger than that for a water/DCE interface, so that the former is likely to construct a molecularly sharp interface. Therefore, interfacial roughness decreases with increasing interfacial tension (Table 3).

In the physical meaning, interfacial roughness is explained in terms of the thermal capillary waves propagating at a water/oil interface, which are related to the interfacial tension of the system.[42–45] It is well established that mean square roughness at a liquid interface can be calculated from a model originally proposed by Buff et al.[42] In essence, any single-valued interface can be described by a Fourier series of interfacial waves. For a liquid surface, the amplitude of each wave is dependent on both the wavelength and the temperature via a Boltzmann distribution. Macroscopic roughness of the interface can be evaluated from the wave amplitude integrated over all relevant wavelengths. The mean squared height ($\langle z^2 \rangle$) is described by the following expression:

$$\langle z^2 \rangle = \frac{k_B T}{4\pi^2} \int_0^{2\pi} \int_0^{k_{max}} \frac{k_r}{\Delta\rho g + \gamma {k_r}^2} \, dk_r \, d\phi \quad (6)$$

Integration of Eq. 6 yields

$$\langle z^2 \rangle = \frac{k_B T}{4\pi\gamma} \ln\left(\frac{\Delta\rho g + \gamma {k^2}_{max}}{\Delta\rho g} \right) \quad (7)$$

where z is the vertical displacement from the mean height, k_r is the magnitude of the radial wavevector for a particular capillary wave within the interfacial plane, ϕ is the azimuth angle of rotation with in the interfacial plane, k_B is the Boltzmann constant, T is the temperature, γ is the surface tension, $\Delta\rho$ is the difference in density between the two media, and g is the gravitational constant. The upper integration limit, k_{max}, describes the largest magnitude of the interfacial wavevector, which is equivalent to the smallest capillary wavelength. Since capillary waves with wavelengths shorter than the intermolecular spacing are not expected to be stable, k_{max} is usually assumed to be in the order of π/r_{min}. In the case of a vapor-liquid interfacial system, r_{min} is the molecular radius of the liquid. In the case of a liquid/liquid interfacial system, r_{min} is assumed to be a weighted mean of the two liquid molecular radii.

The validity of Eq. 7 has been confirmed by means of X-ray reflectivity measurements on roughness at various liquid/vapor interfaces.[115,116] Recently, X-ray reflectivity measurements have been also introduced to study liquid/liquid interfaces.[66–68] Mitrinovic et al. applied X-ray reflectivity to study the electron density profile normal to a water/hexane interface, and estimated interfacial width of a water/hexane interface to be 0.33 ± 0.025 nm, which was in agreement with that predicted from the capillary wave theory.[66] According to Eq. 7, the interfacial width of a water/CCl_4 or water/DCE interface is calculated to be 5 or 6.4 Å, respectively. These values are smaller than the molecular size of SR101 (14 Å). Therefore, the experimental results of three-dimensional molecular rotational reorientation of SR101 and structural dimension larger than 2 at the water/DCE interface could not be explained by the capillary wave theory (Eq. 7). Such a discrepancy between microscopic and macroscopic roughness at a water/oil interface has been discussed by Wirth et al.[76] The thermal capillary wave theory is derived from macroscopic properties at a liquid/liquid interface, so that the theory is not necessarily sufficient to explain interfacial roughness at a molecular level. The applicability of the thermal capillary wave theory has been confirmed for interfacial roughness with tenths of micrometers or larger, and the theory is expected to fail for that in submicrometer length scales.[117]

In order to explain molecular scale interfacial roughness, several theoretical models have been also proposed.[45,118] Rowlen et al. introduced scale-dependent effective roughness, which described the root mean square probability of finding a particular difference in the height between any two points at the interface as a function of lateral separation.[45] Mecke et al. proposed a density functional theory, in which they reconciled the two approaches, by distinguishing the different types of fluctuations at all length scale: both for undulations of the interface and for bulk density fluctuations.[118] They first described an interface as a continuous variation of the density, which is caused by density fluctuations within the bulk phase, but with no undulations of the interfacial position. In the second step, the undulation predicted by the capillary wave theory was taken into account. Recently, the density functional theory was checked experimentally by means of grazing incidence X-ray scattering measurements at an air/water interface.[117] Fradin et al. observed a large decrease in the surface energy of submicrometer waves, up to 75%, that could not be explained by the capillary theory, but was in accord with the effects arising from the non-locality of attractive intermolecular interactions, as predicted by the density functional theory. They also predicted that the surface was rougher than that expected from the simple capillary model at small length scales. Such a density functional theory is not contradicted by our interfacial model: the water/DCE interface is thin (~1 nm), but is rough with respect to the spatial resolution of the excitation energy transfer quenching method (~7 nm, Scheme 3). Furthermore, no clear relationship between the interfacial tension and interfacial roughness could be obtained in this study (Table 3). The results suggest that molecular-scale interfacial roughness would be governed by not only the interfacial tension (as a macroscopic property), but also by the chemical/physical nature of an organic solvent itself. Liquid/liquid interfacial structures would be governed by several factors such as dipole moment, dielectric constant, hydrogen bonding, density, molecular shape of a liquid, and so forth, so that interfacial roughness and nature of a liquid could be correlated in a very complex manner. Further experimental and theoretical studies including molecular dynamic simulations will reveal detailed characteristics at a liquid/liquid interface.

4. A Relationship between Interfacial Structures and Polarity of a Water/Oil Interface

The polarity at a water/oil interface sometimes plays important roles in deciding heterogeneous reaction kinetics.[119] Such results suggest that solvent environments at the interface are different from those in bulk media. In practice, the polarity of interfacial regions such as in microemulsions[120] and micelles[121,122] has been investigated by means of UV/vis absorption spectroscopy on a polarity indicator molecule: 2,6-diphenyl-4-(2,4,6-triphenyl-1-pyridino)phenoxide (DPP). However, these studies do not provide direct information about the inter-

facial polarity, since the experiments are conducted for bulk systems. Recently, surface selective spectroscopic techniques have been applied to studying the polarity at a water/oil interface. As an example, Perera et al. reported the mean polarities at water/heptane, water/decane, and water/cyclohexane interfaces by using attenuated-total-internal reflectance (ATR) absorption spectroscopy. They demonstrated that the absorption peak of DPP at the interface was in the range of 600 ± 10 nm, corresponding to a solvent polarity parameter of $E_T(30) = 47.7 \pm 0.8$ kcal/mol.[119] On the other hand, Bessho et al. applied time-resolved total-internal-reflection (TIR) fluorescence spectroscopy to studying microenvironments around 1-anilino-8-naphthalenesulfonate (ANS) at a water/heptane interface,[83] and they suggested that the interfacial polarity was intermediate between that of heptane and that of water.

As another approach, Wang et al. reported an SHG (second harmonic generation) spectroscopic study on the polarities of water/DCE and water/chlorobenzene (CB) interfaces by using *N*,*N*-diethyl-*p*-nitroaniline (DEPNA) as a probe.[123] According to their study, the interfacial polarity ($P_{A/B}$) is equal to the arithmetic average of the polarities of the adjoining bulk phase (P_A and P_B): Eq. 8.

$$P_{A/B} = \frac{P_A + P_B}{2} \tag{8}$$

They explained the results by dominance of long-range solute-solvent interactions in determining the difference in the excited- and ground-state solvation energies around DEPNA at the interface, but not by local interfacial interactions. The applicability of Eq. 8 was checked for water/heptane, water/decane, and water/cyclohexane systems on the basis of the $E_T(30)$ parameter. However, the variation of $E_T(30)$ by these three solvents was only 1.2 kcal/mol. On the other hand, Michael and Benjamin reported molecular dynamics computer simulations of an electronic spectrum of DEPNA at a water/DCE interface[124] and predicted that the interfacial polarity was influenced by both interfacial roughness and the position of the probe molecule at the interface.[39] In addition to the long-range solute–solvent interaction at the interface, they also demonstrated that short-range solute–solvent interactions were also important in determining the difference in the excited- and ground-state solvation energies around the probe molecule at the interface. Although such studies are very important for advances in the relevant research fields, both experimental and theoretical studies on the polarity at a water/oil interface are still limited. In particular, the applicability of Eq. 8 is worth studying further in a wide range of $E_T(30)$ and the role of interfacial roughness in determining the polarity should be clarified experimentally.

In order to obtain a clearer picture on the interfacial polarity, we conducted picosecond TIR fluorescence spectroscopy by using Sulforhodamine B (SRB) as a polarity probe molecule.[93] Since SRB is surface active and possesses a high fluorescence quantum yield, the dye is very suitable for TIR fluorescence measurements on the polarity at a water/oil interface, as discussed in the preceding sections. Furthermore, it has been reported that the nonradiative decay rate constant (k_{nr}) of a xanthene dye represented by SRB or Rhodamine B (RB) is sensitive to medium polarity and that $\ln(k_{nr})$ is linearly correlated with $E_T(30)$.[125,126] On the basis of fluorescence dynamic measurements of SRB adsorbed on a water/oil interface, therefore, we looked for a relationship between thickness/roughness and the polarity at the interface.

The photophysical properties of a xanthene dye have been extensively studied.[113,125–129] In order to explain a relationship between k_{nr} of the dye and a solvent polarity parameter $E_T(30)$, Quitevis et al. proposed a two-state model.[125,126] In the model, a fluorescent state A^*, which can only decay radiatively to the ground state S_0, is in rapid equilibrium with a non-emissive state B^*, which can only decay to S_0 via internal conversion. According to the model, k_{nr} is given by

$$k_{nr} \propto \exp\{-(\beta/RT + \kappa)(E_T(30) - 30)\}\exp(-\Delta G_{A^*B^*}{}^0/RT) \tag{9}$$

where β and κ are constants and, $\Delta G_{A^*B^*}{}^0$ is the Gibbs free energy difference between A^* and B^* in a non-polar solvent. If Eq. 9 holds, a plot of $\ln k_{nr}$ vs $E_T(30)$ should be linear with the slope value being equal to $-(\beta/RT + \kappa)$. In practice, Quitevis et al. succeeded in explaining solvent effects on the photophysical characteristics of RB in various alcohols and nitriles. The physical meaning of Eq. 9 is not straightforward and it will be better to consider this as an empirical equation. Nonetheless, the relation is useful to explain solvent effects on the spectroscopic properties of a xanthene dye. Therefore, we studied the applicability of the model to the photophysical properties of SRB in water-1,4-dioxane mixtures and in several alcohols.

The fluorescence lifetimes (τ determined at 580 nm) and quantum yields (Φ) of SRB determined in water-dioxane mixtures and a series of alcohols at 25 °C are summarized in Table 4. k_{nr} thus calculated from τ and Φ is also included in Table 4. The k_{nr} value varied with the medium in the range of (4.1–0.7) $\times 10^8$ s^{-1}, whereas the radiative decay rate constant (k_r) was rather insensitive tothe medium properties: (2.8–1.7) $\times 10^8$ s^{-1}. The relationship between $\ln k_{nr}$ and $E_T(30)$ is shown in Fig. 8. As seen clearly, all the data fall on a straight line and the slope

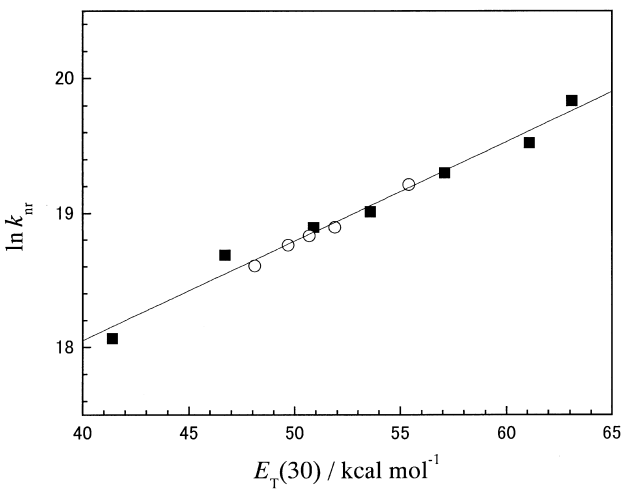

Fig. 8. Relationship between the natural logarithm of k_{nr} (determined in water-1,4-dioxane mixtures (close square) and alcohols (open circle)) and $E_T(30)$. The solid line represents the best fit by using Eq. 9.

Table 4. Photophysical Parameters of SRB in Water–1,4-Dioxane Mixtures and Alcohols

Solvent	$E_T(30)$[a] /kcal mol^{-1}	λ_{em}[b] /nm	τ /ns	k_r /10^8 s^{-1}	k_{nr} /10^8 s^{-1}	Φ[c]
H_2O:Dioxane /vol%						
100:0	63.1	583	1.50	2.61	4.08	0.39
90:10	61.1	584	1.75	2.78	2.95	0.49
70:30	57.1	583	2.07	2.46	2.37	0.51
50:50	53.6	582	2.33	2.54	1.76	0.59
30:70	50.9	579	2.56	2.33	1.58	0.60
10:90	46.7	576	2.85	2.20	1.31	0.63
2:98	41.4	569	3.38	2.24	0.72	0.79
Alcohol[d]						
MeOH	55.4	574	2.33	2.06	2.24	0.48
EtOH	51.9	572	2.83	1.94	1.63	0.55
PrOH	50.7	570	3.13	1.73	1.47	0.54
BuOH	49.7	570	3.20	1.68	1.44	0.54
OctaOH	48.1	572	3.21	1.90	1.21	0.61

a) The value is calculated on the basis of a volume percentage of 1,4-dioxane in H_2O.
b) The fluorescence maximum wavelength of SRB.
c) The fluorescence quantum yield of SRB relative to the value in ethanol.
d) MeOH, EtOH, PrOH, BuOH, and OctaOH represent methanol, ethanol, 1-propanol, 1-butanol, and 1-octanol, respectively.

Table 5. Photophysical Parameters of SRB and Polarities at the Water/Oil Interfaces

Org. Phase	$E_T(30)$[a] /kcal mol^{-1}	τ /ns	k_{nr} /10^8 s^{-1}	$E_T(30)_{int}$ /kcal mol^{-1}	$E_T(30)_{calc}$ /kcal mol^{-1}
Cyclohexane	30.9	3.00	1.13	46.7	47.0
CCl_4	32.4	2.95	1.18	47.4	47.8
Toluene	33.9	2.84	1.32	48.8	48.5
CB	36.8	2.89	1.25	48.1	50.0
DCB	38.0	3.00	1.13	46.7	50.6
DCE	41.3	2.78	1.39	49.5	52.2

a) The value for the oil.

value of the plot was 0.074 ± 0.01. Although the slope value is somewhat smaller than that determined for RB in alcohols (0.12 ± 0.02),[125] the photophysical properties of SRB and Eq. 9 are applicable to probing the polarity at a water/oil interface.

Figure 7 shows the fluorescence decay profiles of SRB at a water/DCE interface and in an aqueous solution, together with the relevant *Re* for each single-exponential fit. Analogous results were obtained for other water/oil systems (data are not shown), and the τ values determined are summarized in Table 5. It is noteworthy that the TIR fluorescence decay curve observed at each water/oil interface is reasonably fitted by a single-exponential function as judged by *Re*, and their lifetime is always longer than that in an aqueous phase (1.5 ns). Table 4 indicates that k_r is not sensitive to solvent environments compared to k_{nr}. Assuming k_r to be constant at the average value (2.21×10^8 s^{-1}) of those in the bulk solutions (Table 4), we calculated k_{nr} of SRB at the interface: $k_{nr} = \tau^{-1} - k_r$. The interfacial polarity $E_T(30)_{int.}$ in each water/oil system was then estimated on the basis of the relevant k_{nr} value and the relationship in Fig. 8. The results are summarized in Table 5 and Fig. 9, together with interfacial polarity $E_T(30)_{calc}$ calculated by Eq. 8. These data demonstrate that $E_T(30)_{int}$ observed takes always

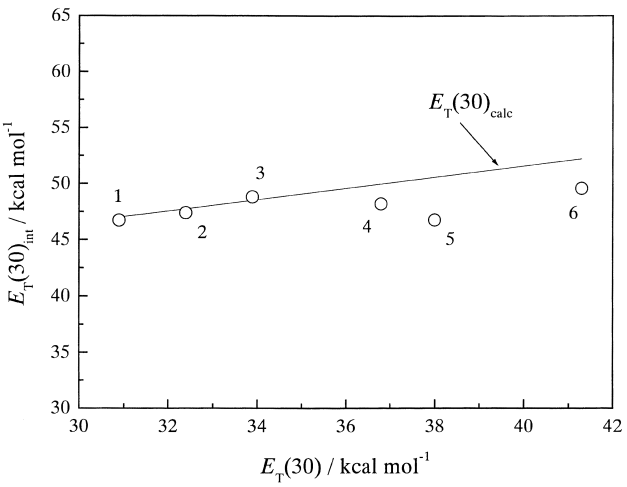

Fig. 9. Relationship between $E_T(30)_{int}$ and $E_T(30)$ of the oil phase. Open circles and solid curve represent $E_T(30)_{int}$ and $E_T(30)_{calc}$, respectively. 1: cyclohexane, 2: carbon tetrachloride, 3: toluene, 4: chlorobenzene, 5: *o*-dichlorobenzene, 6: 1,2-dichloroethane.

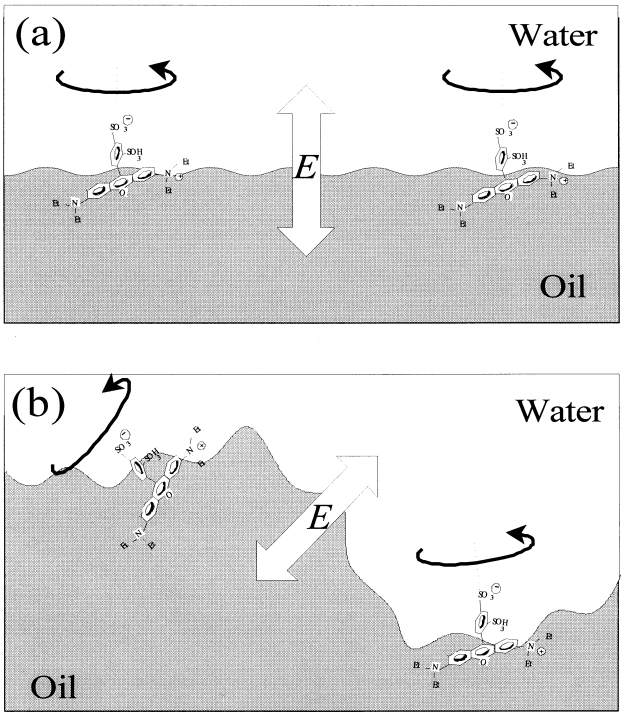

Fig. 10. Schematic illustrations of sharp ((a)) and rough ((b)) water/oil interfaces. *E* denotes the direction of the electric field generated across the water/oil interface. The arrows represent the rotational reorientation of SRB at the water/oil interfaces.

an intermediate value between $E_T(30)$ of water and that of the organic phase. In the case of a relatively low polarity solvent (cyclohexane, CCl_4, or toluene), $E_T(30)_{int}$ agreed very well with $E_T(30)_{calc}$ as predicted by Eq. 8. In these interfacial systems, our fluorescence data indicate that the interface is thin and two-dimension-like. When a water/oil interface is thin and sharp, therefore, it is concluded that the interfacial polarity is well predicted by the arithmetic average of the polarities of the water and organic phases: Eq. 8. In the case of a relatively high polarity solvent (CB, *o*-DCB, or DCE), on the other hand, $E_T(30)_{int.}$ was always lower than $E_T(30)_{calc}$. The time resolution of our experimental setup is 20 ps and k_r of the dye is rather insensitive to a solvent polarity compared to k_{nr}, so that we think that the deviation of $E_T(30)_{int}$ from $E_T(30)_{calc}$ in these systems is meaningful. It is worth noting that these water/oil interfaces are thin (~1 nm) but rough (in the spatial resolution of R_0) as estimated by the fluorescence dynamic spectroscopies: dynamic anisotropy and energy transfer method. The results demonstrate that an interfacial polarity deviates from $E_T(30)_{calc}$ when the interface is rough. We suppose that the origin of the present results would be due to interfacial roughness and orientations of SRB adsorbed on the interface, as discussed below.

The observed interfacial polarity agrees roughly with $E_T(30)_{calc}$ irrespective of the experimental method (SHG,[123] ATR absorption,[119] TIR fluorescence[93]) or of the probe molecule used (DEPNA,[123] DPP,[119] SRB[93]). Therefore, we conclude that the interfacial polarity is governed predominantly by long-range dipole–dipole interactions between solute and solvent molecules. For a flat and sharp interface such as water/cyclohexane, water/CCl_4 or water/toluene, two-dimensional-like rotational freedom of the dye indicates that an orientational distribution of the probe molecule at the interface is narrow, as schematically illustrated in Fig. 10a, where the dye is adsorbed on the interface with the long axis of the xanthene ring being tilted about 70° to surface normal, while the $-SO_3^-$ group of the dye is directed to the water phase as reported previously.[86] Therefore, the dipole moment governing the photophysical characteristics of SRB at the interface would align with respect to surface normal. Under such a circumstance, if the electric field generated across the water/oil interface stabilizes the dipole of the probe molecule, the interfacial polarity would be observed as the arithmetic average of the polarities of the two phases (Eq. 8) owing to the almost uniform distribution of SRB at the interface. On the other hand, a rough interface would render a relatively random distribution of the dipole moment of the dye (Fig. 10b) compared to that at a sharp/flat interface. The rough interface also leads to randomization of the direction of the electric field at the interface. As the result, the probe molecule adsorbed on the rough interface would be less influenced by the electric field, leading to the interfacial polarity being smaller than $E_T(30)_{calc}$. At the present stage of the investigation, these pictures are speculative and there is no theoretical background. Nonetheless, we think that such an idea will be one of the possible explanations for the present results on the relation between the polarity and roughness/thickness of the interface.

Conclusions

In order to obtain structural information about water/oil interfaces at a molecular level, two different approaches were introduced to the study. One is a magic angle dependence of the TIR fluorescence decay profile of SR101 adsorbed on a water/oil interface. The other approach was a structural dimension analysis of excitation energy transfer dynamics between dye molecules adsorbed on water/oil interfaces. The latter method was shown to have high potential to elucidate the thickness and roughness of the interfacial layer in the spatial resolution of the critical energy transfer distance (~7 nm) between an energy donor and an acceptor. By using these two methods, we demonstrated that a water/CCl_4 interface was very sharp with respect to molecular dimension of SR101. On the other hand, a water/DCE interface was concluded to be rougher than a water/CCl_4 interface. It is worth noting that the present results are the first experimental proof of the structural difference between the water/CCl_4 and water/DCE interfaces. These approaches are very meaningful in respect to comparative discussion on the same systems by both experiments and available computer simulation data by Benjamin and co-workers. Furthermore, it has been suggested that roughness of the water/DCE interface is caused by thermal fluctuation of the sharp (~1 nm) interface in the range of ~7 nm.

These methodologies were also extended to study other water/oil interfacial systems with the properties of the oil being varied. Such a systematic study on water/oil interfaces has been rarely explored up to now and, therefore, the present study contributes to further advances in the relevant researches. Systematic investigations on water/oil interfaces are the

first step to reveal factors governing structural and physical characteristics of the interfaces. Usually, interfacial roughness is explained in terms of the thermal capillary waves propagating at the interface, which are related to interfacial tension of the system. However, the thermal capillary wave theory has been derived from macroscopic properties at a liquid/liquid interface, so that the theory is not necessarily sufficient to explain interfacial roughness at a molecular level. Actually, no clear relationship between interfacial tension and interfacial roughness could be obtained in the present study. The results clearly suggest that molecular-scale interfacial roughness would be governed not only by interfacial tension (as a macroscopic property), but also by the chemical/physical nature of an organic solvent itself.

Various chemical processes *at* or *across* liquid/liquid interfaces are governed by the molecular level structures of the interfaces. In this article, we discussed the relationship between interfacial thickness/roughness and the nature of an oil phase for the first time. Also, the present study suggested that interfacial roughness would govern various reaction processes across a liquid/liquid interface. In separation sciences, such the process is very important: typical examples are solvent extraction and liquid chromatography. Although the present study is focused on flat water/oil interfaces, the results and methodologies introduced by the study will contribute to further researches in the chemistry at liquid/liquid interfaces.

This work was supported by a Grant-in-Aid from the Ministry of Education, Science, Sports and Culture (No. 11740404 to S.I.). N.K. is grateful for a Grant-in-Aid from the Ministry of Education, Science, Sports, and Culture, for the Priority Research Area B on "Laser Chemistry of Single Nanometer Organic Particles" (No. 10207201) for partial support of this research.

References

1 Y. Surakitbanharn, S. Muralidharan, and H. Freiser, *Anal. Chem.*, **63**, 2642 (1991).
2 E. V. Demlow and S. S. Demlov, "Phase Transfer Catalysis," 2nd revised edition, Verlag Chemie, Weinheim (1983).
3 H. Watarai, *Bunseki Kagaku*, **45**, 725 (1996).
4 H. H. Girault and D. J. Schiffrin, in "Electroanalytical Chemistry," A. J. Bard, Ed., Marcel Dekker, New York (1989) , Vol. 15, Chapter 1.
5 "Liquid-Liquid Interfaces," ed by A. G. Volkov, and D. W. Deamer, CRC Press: Boca Raton, FL (1996).
6 H. H. Girault, *Electrochim. Acta*, **32**, 383 (1987).
7 T. Wandlowski, V. Marecek, K. Holub, and Z. Samec, *J. Phys. Chem.*, **93**, 8204 (1989).
8 K. Nakatani, K. Chikama, H.-B. Kim, and N. Kitamura, *Chem. Lett.*, **4**, 793 (1994).
9 K. Nakatani, T. Suto, M. Wakabayashi, H.-B. Kim, and N. Kitamura, *J. Phys. Chem.*, **99**, 4745 (1995).
10 K. Nakatani, K. Chikama, H.-B. Kim, and N. Kitamura, *Chem. Phys. Lett.*, **237**, 133 (1995).
11 K. Nakatani, N. Terui, and N. Kitamura, *Bull. Chem. Soc. Jpn.*, **69**, 997 (1996).
12 K. Nakatani, M. Wakabayashi, K. Chikama, and N. Kitamura, *J. Phys. Chem.*, **100**, 6749 (1996).
13 K. Nakatani, N. Terui, K. Hasebe, and N. Kitamura, *Chem. Lett.*, **6**, 457 (1996).
14 K. Chikama, K. Nakatani, and N. Kitamura, *Chem. Lett.*, **6**, 665 (1996).
15 K. Nakatani, M. Sudo, and N. Kitamura, *J. Phys. Chem. B*, **102**, 2908 (1998).
16 K. Chikama, K. Nakatani, and N. Kitamura, *Bull. Chem. Soc. Jpn.*, **71**, 1065 (1998).
17 K. Nakatani, M. Sudo, and N. Kitamura, *Anal. Chem.*, **72**, 339 (2000).
18 N. Terui, K. Nakatani, and N. Kitamura, *J. Electroanal. Chem.*, **494**, 41 (2000).
19 L. Troxler and G. Wipff, *Anal. Sci.*, **14**, 43 (1998).
20 T. Shioya, S. Nishizawa, and N. Teramae, *J. Am. Chem. Soc.*, **120**, 11534 (1998).
21 N. Muzet, E. Engler, and G. Wipff, *J. Phys. Chem. B*, **102**, 10772 (1998).
22 T. Kakiuchi and M. Senda, *Bull. Chem. Soc. Jpn.*, **56**, 2912 (1983).
23 H. H. Girault and D. J. Schiffrin, *J. Electroanal. Chem.*, **170**, 127 (1984).
24 T. Kakiuchi, M. Nakanishi, and M. Senda, *Bull. Chem. Soc. Jpn.*, **61**, 1845 (1988).
25 Y. Chiba and H. Watarai, *Bull. Chem. Soc. Jpn.*, **69**, 341 (1996).
26 H. Nagatani and H. Watarai, *Anal. Chem.*, **68**, 1250 (1996).
27 H. Nagatani and H. Watarai, *Chem. Lett.*, **2**, 167 (1997).
28 H. Nagatani and H. Watarai, *J. Chem. Soc., Faraday Trans.*, **94**, 247 (1998).
29 Y. Onoe, S. Tsukahara, and H. Watarai, *Bull. Chem. Soc. Jpn.*, **71**, 603 (1998).
30 H. Nagatani and H. Watarai, *Anal. Chem.*, **70**, 2860 (1998).
31 H. Nagatani and H. Watarai, *Chem. Lett.*, **7**, 701 (1999).
32 R. D. Webster, R. A. W. Dryfe, B. A. Coles, and R. G. Compton, *Anal. Chem.*, **70**, 792 (1998).
33 I. Benjamin, *J. Chem. Phys.*, **97**, 1432 (1992).
34 I. Benjamin, *Science*, **261**, 1558 (1993).
35 D. Michael and I. Benjamin, *J. Phys. Chem.*, **99**, 1530 (1995).
36 K. J. Schweighofer and I. Benjamin, *J. Phys. Chem.*, **99**, 9974 (1995).
37 D. Michael and I. Benjamin, *J. Phys. Chem.*, **99**, 16810 (1995).
38 I. Benjamin, *Chem. Rev.*, **96**, 1449 (1996).
39 D. Michael and I. Benjamin, *J. Chem. Phys.*, **107**, 5684 (1997).
40 T.-M. Chang and L. X. Dang, *J. Chem. Phys.*, **108**, 818 (1998).
41 K. J. Schweighofer and I. Benjamin, *J. Chem. Phys.*, **112**, 1474 (2000).
42 F. P. Buff, R. A. Lovett, and F. H. Stillinger, Jr., *Phys. Rev. Lett.*, **15**, 621 (1965).
43 A. Braslau, P. S. Pershan, G. Swislow, B. M. Ocko, and J. Als-Nielsen, *Phys. Rev. A*, **38**, 2457 (1988).
44 P. S. Pershan, *Faraday Discuss. Chem. Soc.*, **89**, 231 (1990).
45 G. J. Simpson and K. L. Rowlen, *Chem. Phys. Lett.*, **309**, 117 (1999).
46 S. G. Grubb, M. W. Kim, T. Rasing, and Y. R. Shen, *Langmuir*, **4**, 452 (1988).
47 J. C. Conboy, J. L. Daschbach, and G. L. Richmond, *J. Phys. Chem.*, **98**, 9688 (1994).

48 J. C. Conboy, J. L. Daschbach, and G. L. Richmond, *Appl. Phys. A-Solids & Surfaces*, **59**, 623 (1994).
49 J. C. Conboy and G. L. Richmond, *Electrochim. Acta*, **40**, 2881 (1995).
50 M. J. Carwford, J. G. Frey, T. J. Vandernoot, and Y. G. Zhao, *J. Chem. Soc., Faraday Trans.*, **92**, 1369 (1996).
51 R. R. Naujok, H. J. Paul, and R. M. Corn, *J. Phys. Chem.*, **100**, 10497 (1996).
52 J. Rinuy, A. Piron, P. F. Brevet, D. M. Blanchard, and H. H. Girault, *Chemistry-A Eur. J.*, **6**, 3434 (2000).
53 R. M. Corn and D. A. Higgins, *Chem. Rev.*, **94**, 107 (1994).
54 Q. Du, E. Freysz, and Y. R. Shen, *Science*, **264**, 826 (1994).
55 M. C. Messmer, J. C. Conboy, and G. L. Richmond, *J. Am. Chem. Soc.*, **117**, 8039 (1995).
56 J. C. Conboy, M. C. Messmer, and G. L. Richmond, *J. Phys. Chem.*, **100**, 7617 (1996).
57 R. A. Walker, J. C. Conboy, and G. L. Richmond, *Langmuir*, **13**, 3070 (1997).
58 J. C. Conboy, M. C. Messmer, and G. L. Richmond, *J. Phys. Chem. B*, **101**, 6724 (1997).
59 D. E. Gragson, J. C. Conboy, and G. L. Richmond, *Langmuir*, **13**, 4804 (1997).
60 D. E. Gragson and G. L. Richmond, *J. Phys. Chem. B*, **102**, 569 (1998).
61 D. E. Gragson and G. L. Richmond, *J. Am. Chem. Soc.*, **120**, 366 (1998).
62 R. A. Walker, J. A. Gruetzmacher, and G. L. Richmond, *J. Am. Chem. Soc.*, **120**, 6991 (1998).
63 R. A. Walker, D. E. Gragson, and G. L. Richmond, *Colloids & Surf. A-Phys. & Eng. Aspects*, **154**, 175 (1999).
64 B. L. Smiley and G. L. Richmond, *Biopolymers*, **57**, 117 (2000).
65 M. G. Brown, E. A. Raymond, H. C. Allen, L. F. Scatena, and G. L. Richmond, *J. Phys. Chem. A*, **104**, 10220 (2000).
66 D. M. Mitrinovic, Z. Zang, S. M. Williams, Z. Huang, and M. L. Schlossman, *J. Phys. Chem. B*, **103**, 1779 (1999).
67 A. M. Tikhonov, D. M. Mitrinovic, M. Li, Z. Huang, and M. L. Schlossman, *J. Phys. Chem. B*, **104**, 6336 (2000).
68 D. M. Mitrinovic, A. M. Tikhonov, M. Li, Z. Huang, and M. L. Schlossman, *Phys. Rev. Lett.*, **85**, 582 (2000).
69 Z. H. Zhang, I. Tsuyumoto, S. Takahashi, T. Kitamori, and T. Sawada, *J. Phys. Chem. A*, **101**, 4163 (1997).
70 S. Takahashi, I. Tsuyumoto, T. Kitamori, and T. Sawada, *Electrochim. Acta*, **44**, 165 (1998).
71 I. Tsuyumoto, N. Noguchi, T. Kitamori, and T. Sawada, *J. Phys. Chem. B*, **102**, 2684 (1998).
72 Y. Uchiyama, I. Tsuyumoto, T. Kitamori, and T. Sawada, *J. Phys. Chem. B*, **103**, 4663 (1999).
73 Y. Uchiyama, M. Fujinami, T. Sawada, and I. Tsuyumoto, *J. Phys. Chem. B*, **104**, 4699 (2000).
74 Y. Uchiyama, T. Kitamori, T. Sawada, and I. Tsuyumoto, *Langmuir*, **16**, 6597 (2000).
75 L. E. Morrison and G. Weber, *Biophys. J.*, **52**, 367 (1987).
76 M. J. Wirth and J. D. Burbage, *J. Phys. Chem.*, **96**, 9022 (1992).
77 J. M. Kovaleski and M. J. Wirth, *J. Phys. Chem.*, **99**, 4091 (1995).
78 J. M. Kovaleski and M. J. Wirth, *J. Phys. Chem.*, **100**, 10304 (1996).
79 H. Watarai and Y. Saitoh, *Chem. Lett.*, **4**, 283 (1995).
80 R. Okamura, T. Hinoue, and H. Watarai, *Anal. Sci.*, **12**, 393 (1996).
81 K. Nakatani, S. Ishizaka, and N. Kitamura, *Anal. Sci.*, **12**, 701 (1996).
82 H. Watarai and F. Funaki, *Langmuir*, **12**, 6717 (1996).
83 K. Bessho, T. Uchida, A. Yamauchi, T. Shioya, and N. Teramae, *Chem. Phys. Lett.*, **264**, 381 (1997).
84 Y. Saitoh and H. Watarai, *Bull. Chem. Soc. Jpn.*, **70**, 351 (1997).
85 S. Tsukahara and H. Watarai, *Langmuir*, **14**, 7072 (1998).
86 S. Ishizaka, K. Nakatani, S. Habuchi, and N. Kitamura, *Anal. Chem.*, **71**, 419 (1999).
87 S. Ishizaka, S. Habuchi, H.-B. Kim, and N. Kitamura, *Anal. Chem.*, **71**, 3382 (1999).
88 S. Tsukahara and H. Watarai, *Chem. Lett.*, **1**, 89 (1999).
89 M. Fujiwara, S. Tsukahara, and H. Watarai, *Phys. Chem. Chem. Phys.*, **1**, 2949 (1999).
90 H. Nagatani, R. A. Iglesias, D. J. Fermin, R. F. Brevet, and H. H. Girault, *J. Phys. Chem. B*, **104**, 6869 (2000).
91 M. A. Jones and P. W. Bohn, *Anal. Chem.*, **72**, 3776 (2000).
92 S. Tsukahara, Y. Yamada, and H. Watarai, *Langmuir*, **16**, 6787 (2000).
93 S. Ishizaka, H.-B. Kim, and N. Kitamura, *Anal. Chem.*, **73**, 2421 (2001).
94 J. A. Riddick and W. B. Bunger, "Techniques of Chemistry: Organic Solvents," Wiley-Interscience, New York (1970), Vol. II.
95 D. V. O'Connor and D. Phillips, "Time-Correlated Single Photon Counting," Academic Press, New York (1986).
96 M. J. Wirth and J. D. Burbage, *Anal. Chem.*, **63**, 1311 (1991).
97 R. L. Christensen, R. C. Drake, and D. Phillips, *J. Phys. Chem.*, **90**, 5960 (1986).
98 E. V. Sitzmann and K. B. Eisenthal, *J. Chem. Phys.*, **90**, 3831 (1989).
99 a) J. Klafter and A. Blumen, *J. Chem. Phys.*, **80**, 875 (1984). b) J. Klafter and A. Blumen, *J. Lumin.*, **34**, 77 (1985).
100 N. Tamai, T. Yamazaki, and I. Yamazaki, *Chem. Phys. Lett.*, **147**, 25 (1988).
101 I. Yamazaki, N. Tamai, and T. Yamazaki, *J. Phys. Chem.*, **94**, 516 (1990).
102 N. Tamai, T. Yamazaki, I. Yamazaki, A. Mizuma, and N. Mataga, *J. Phys. Chem.*, **91**, 3503 (1987).
103 Y. Lin, M. C. Nelson, and D. M. Hanson, *J. Chem. Phys.*, **86**, 1586 (1987).
104 O. Tcherkasskaya, J. G. Spiro, S. Ni, and M. A. Winnik, *J. Phys. Chem.*, **100**, 7114 (1996).
105 A. Yekta, J. G. Spiro, and M. A. Winnik, *J. Phys. Chem. B*, **102**, 7960 (1998).
106 H.-B. Kim, S. Habuchi, and N. Kitamura, *Anal. Chem.*, **71**, 842 (1999).
107 D. Rojanski, D. Huppert, H. D. Bale, X. Dacai, P. W. Schmidt, D. Farin, A. Seri-Levy, and D. Avnir, *Phys. Rev. Lett.*, **56**, 2505 (1986).
108 P. Levitz and J. M. Drake, *Phys. Rev. Lett.*, **58**, 686 (1987).
109 D. Rojanski, D. Huppert, and D. Avnir, *Chem. Phys. Lett.*, **139**, 109 (1987).
110 Th. Förster, *Discuss. Faraday Soc.*, **27**, 7 (1959).
111 The following values were used to calculate the R_0 value: $\phi_0 = 1.00$,[29] n (water) $= 1.33$,[30] and $\int_0^\infty F_D(\nu)\varepsilon_A(\nu)/\nu^4 d\nu = 7.0 \times 10^{-13}$.
112 W. Adamson, "Physical Chemistry of Surfaces," John Wiley and Sons, New York (1990).
113 T. Karstens and K. J. Kobs, *Phys. Chem.*, **84**, 1871 (1980).

114 J. N. Israelachvili, "Intermolecular and Surface Forces," Academic Press Ltd. (1992).
115 A. Braslau, M. Deutsch, P. S. Pershan, and A. H. Weiss, *Phys. Rev. Lett.*, **54**, 114 (1985).
116 M. K. Sanyal, S. K. Sinha, K. G. Huang, and B. M. Ocko, *Phys. Rev. Lett.*, **66**, 628 (1991).
117 C. Fradin, A. Braslau, D. Luzet, D. Smilgies, M. Alba, N. Boudet, K. Mecke, and J. Daillant, *Nature*, **403**, 871 (2000).
118 K. R. Mecke and S. Dietrich, *Phys. Rev. E*, **59**, 6766 (1999).
119 J. M. Perera, G. W. Stevens, and F. Grieser, *Colloids Surf. A*, **95**, 185 (1995).
120 K. A. Zachariasse, N. V. Phuc, and B. Kozankiewicz, *J. Phys. Chem.*, **85**, 2676 (1981).
121 C. J. Drummond, F. Grieser, and T. W. Healy, *Faraday Discuss. Chem. Soc.*, **81**, 95 (1986).
122 G. G. Warr and D. F. Evans, *Langmuir*, **4**, 217 (1988).
123 H. Wang, E. Borguet, and K. B. Eisenthal, *J. Phys. Chem. B*, **102**, 4927 (1998).
124 D. Michael and I. Benjamin, *J. Phys. Chem. B*, **102**, 5145 (1998).
125 K. G. Casey and E. L. Quitevis, *J. Phys. Chem.*, **92**, 6590 (1988).
126 K. G. Casey, Y. Onganer, and E. L. Quitevis, *J. Photochem. Photobiol. A: Chem.*, **64**, 307 (1992).
127 I. Lopez Arbeloa and K. K. Rohatgi-Mukherjee, *Chem. Phys. Lett.*, **128**, 474 (1986).
128 I. Lopez Arbeloa and K. K. Rohatgi-Mukherjee, *Chem. Phys. Lett.*, **129**, 607 (1986).
129 T.-L. Chang and W. L. Borst, *J. Chem. Phys.*, **93**, 4724 (1990).

Shoji Ishizaka was born in 1972 in Hokkaido Prefecture, Japan. He received his B. of Science degree in 1995, his M. of Science degree in 1997, and his Ph.D. in 2001 from Hokkaido University. Now he is a research associate of the Division of Chemistry, Graduate School of Science, Hokkaido University. He engages in time-resolved total internal reflection fluorescence spectroscopy at a liquid/liquid interface to evaluate chemical and structural characteristics at the interface.

Noboru Kitamura was born in 1953 in Tokyo, Japan. He received his B. Eng. degree in 1976 from Tokyo Metropolitan University and, M. Sci. in 1978 and D. Sci. in 1983 both from Tokyo Institute of Technology. He was a research associate of Tokyo Institute of Technology from 1978 to 1988. After spending in the Microphotoconversion Project, ERATO, JST as a technical manager (1988–1993), he is now Professor of the Division of Chemistry, Graduate School of Science, Hokkaido University. His research interests include analytical- and photo-chemistry in minute dimensions, laser spectroscopy, and photochemistry of coordination compounds. For the above academic activities, the Chemical Society of Japan awarded him a prize in 1999.